Journal of Structural Geology 31 (2009) 150–162

Contents lists available at ScienceDirect

Journal of Structural Geology

journal homepage: www.elsevier.com/locate/jsg

Constraints on the depth, geometry and kinematics of blind detachment faults provided by fault-propagation folds: An example from the Mesozoic fold belt of South China

Dan-Ping Yan [a,b,*], Bing Zhang [a], Mei-Fu Zhou [b], Guoqing Wei [a], Hong-Lin Song [a], Shao-Feng Liu [a]

[a] State Key Laboratory for Geological Processes and Mineral Resources and Key Laboratory of Lithospheric Tectonics and Lithoprobing Technology of Ministry of Education, China University of Geosciences, Beijing 100083, China
[b] Department of Earth Sciences, University of Hong Kong, Hong Kong SAR, China

ARTICLE INFO

Article history:
Received 7 March 2008
Received in revised form
14 October 2008
Accepted 6 November 2008
Available online 27 November 2008

Keywords:
Mesozoic fold belt
Fault geometry
Fold parameter
Blind thrust fault
Out-of-sequence and in-sequence duplex
South China

ABSTRACT

The Mesozoic multi-layered thin-skinned, fault-related fold belt in South China is characterized by propagation chevron folding and thrust faulting. We examine the geometry and depth of blind detachment faults in this belt using faults and folds that crop out along a well-defined cross-section. A combination of parameters such as backlimb dip angle (2θ), interlimb angle (γ), height of anticline (h), thickness of the referenced layer (h_0), width of the anticline (AB) and thickness-change ratio of layering within the forelimb (t_f/t) are used to develop new equations to estimate the geometry and depth of the detachment faults. In the cross-section, the Huangdushan chevron anticline has parameters revealing a blind fault with a ramp angle of 42° and a flattened segment at a depth of 4.9 km. Based on existing seismic data, we interpret this blind fault as a backthrust developed over an in-sequence imbricated duplex of Cambrian to Ordovician strata. A chevron anticline at Qiyueshan also reveals a backthrust fault. However, a broad anticline in Lengzhuba and a small cylindrical, sinusoidal anticline in Yupize reveal a flat-ramp-flat detachment fault with flat segments at depths of 7.4 and 3.4 km, respectively, suggesting that the Sinian strata were thickened probably by an out-of-sequence imbricated duplex.

Our results indicate that the flat-ramp-flat detachment fault along the bottom of the Sinian strata produced the out-of-sequence imbricated duplex and cylindrical sinusoidal folds. The in-sequence imbricated duplex produced backthrusts and related chevron anticlines. We consider that this fault-related fold belt was produced by collision between the Yangtze Block and North China Blocks.

1. Introduction

Is there a single detachment level or are there multiple detachment levels? Several geometric and kinematic models of fault-related folds have been developed to predict the variable geometry of detachment faults (Suppe, 1983; Suppe and Medwedeff, 1984, 1990; Jamison, 1987; Chester and Chester, 1990; Mitra, 1990; McNaught and Mitra, 1993; Wickham, 1995; Allmendinger and Shaw, 2000). The primary role of these models is to generate a fault geometry that closely resembles that of natural structures. Geometrical models, which utilize continuum mechanics to simulate deformation, have been used to examine folds associated with fault ramp tips (e.g. Cooke and Pollard, 1997; Johnson and Johnson, 2001) and flat-ramp-flat geometry (e.g. Berger and Johnson, 1980; Kilsdonk and Fletcher, 1989; Strayer and Hudleston, 1997). Kinematic models, which balance the geometry of the deforming system with the undeformed system without incorporating force or rheology, have been used extensively to study fault-bend folding (e.g. Suppe, 1983; Wilkerson et al., 1991; Salvini and Storti, 2001). Both geometric and kinematic models predict that fold shape is dependent, at least in part, upon fault geometry (David et al., 1997; Savage and Cooke, 2003), and thus have been used to analyze fault-related folds. However, previous studies focused on separate or several selected fold parameters associated with detachment faults. In most studies based on surface geology, the relationships between recognizable fold parameters, blind fault geometry and the depth of detachment faults are poorly constrained. Thus, it is difficult to determine the exact geometry and the depth of the multiple level detachment faults.

The well-exposed, thin-skinned, fault-related fold belt in South China is characterized by chevron anticline (box syncline)-thrust

* Corresponding author. School of Earth Sciences and Resources, China University of Geosciences, 29# Xueyuan Road, Beijing 100083, China. Tel.: +86 10 82320225; fax: +86 10 82322226.
E-mail address: yandp@cugb.edu.cn (D.-P. Yan).

0191-8141/$ – see front matter © 2008 Elsevier Ltd. All rights reserved.
doi:10.1016/j.jsg.2008.11.005

fault deformation in the northwest and chevron syncline (box anticline)-thrust fault deformation in the southeast (Fig. 1A). Yan et al. (2003a) proposed a model involving progressive deformation of the thin-skinned tectonic belt in a northwestward and upward stepwise fashion. In this model, formation of a basal detachment fault along the lower part of the Sinian strata (Fz) was followed by shallower detachment faults along the basal contacts of the Cambrian (Fc), Silurian (Fs) and Triassic (Ft) strata. Related folds from chevron anticline to chevron syncline are present (Yan et al., 2003a). However, the detachment faults predicted in this model remain blind and thus their geometry and depth need to be determined using the parameters of exposed folds.

Based on field and seismic data of the fault-propagation folds, we develop equations to constrain the geometry and depth of various detachment faults utilizing fold parameters, and apply these to investigate the fold–fault relationships in a geological section Gc–Gc′ in the thin-skinned fault-related fold belt (Fig. 2). We describe a multi-layer detachment fault–fold system and propose a possible kinematic model for the formation of such a system.

2. Geological background

The Mesozoic multi-layer, thin-skinned, fault-related fold belt in South China occurs in the northwestern part of the Yangtze Block. To the north, the Yangtze Block is separated from the North China Block by the late Paleozoic to early Mesozoic Qingling-Dabie orogenic belt (Zhang et al., 1996, 2006; Liu et al., 2005; Xiao and He, 2005), and to the west from the Mesozoic–Cenozoic Songpan-Ganze orogenic belt by the Longmenshan-Yanyuan thrust belt (Zhou et al., 2002, 2008; Yan et al., 2003b, 2008) (Fig. 1A).

The Banxi Group and its equivalents of Meso- to Neoproterozoic age in the Yangtze Block comprise the metamorphic basement and consist of a well-bedded greywacke-slate succession (Liu et al., 1996; Yan et al., 2003a, 2006; Zhang et al., 2008). The sedimentary cover consists mainly of folded Paleozoic and Lower Mesozoic strata of shallow-marine origin, and tightly folded Sinian strata consisting of tillites and limestones. The Sinian strata are overlain, in succession, by Cambrian strata of black shale, sandstone and limestone interbedded with dolostone, thick-bedded Ordovician limestone interlayered with dolostone and argillaceous siltstone, Silurian shale and fine-grained sandstone, Devonian sandstone, siltstone and sandy shale, Carboniferous clastic rocks and limestones, and Permian carbonate-rich rocks. The Triassic strata include thin layers of limestone interbedded with marl and shale. Jurassic, Cretaceous and Cenozoic strata are composed entirely of continental clastic sequences (HBGMR2, 1988; HBGMR1, 1990; SBGMR, 1991).

The Sichuan Basin in the northwestern part of the Yangtze Block is separated from the Mesozoic fold belt by the Huayun

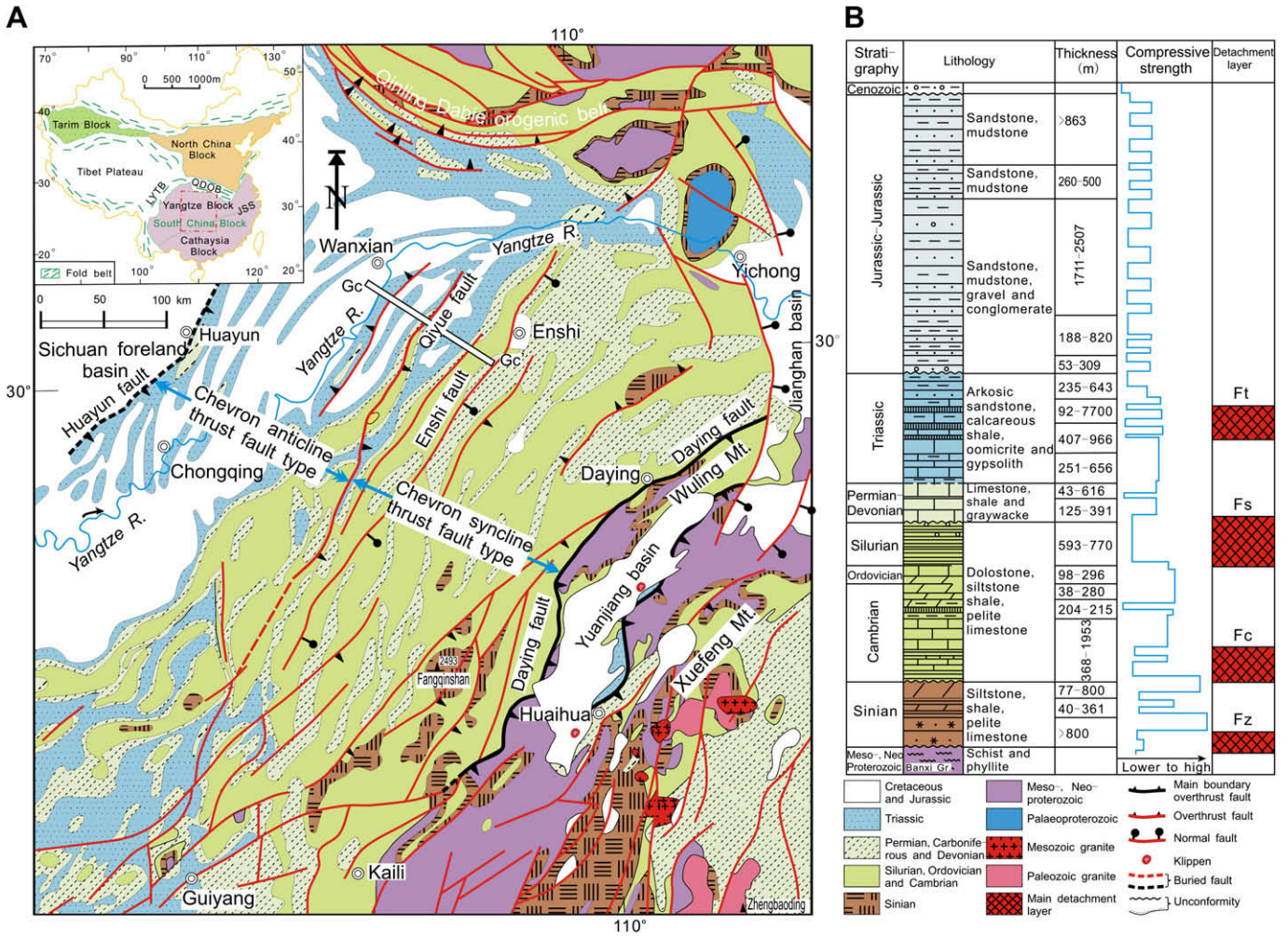

Fig. 1. (A) Structural map of the Yangtze Block, South China, compiled from the following maps: HBGMR1 (1990), HBGMR2 (1988) and SBGMR (1991); (B) columnar section showing the major lithologies, thicknesses, compressive strengths, and possible layers that may develop detachment faults (after Lu et al., unpublished report; SBGMR, 1991; Yan et al., 2003a; Zhang et al., 1996). QDOB: Qingling-Dabie Orogenic Belt; LYTB: Longmenshan-Yanyuan thrust belt; JSS: Jiangshan-Shaoxing Suture Zone. Ft, Fs, Fc and Fz indicate main detachment layer. White bar is trip map of Fig. 2.

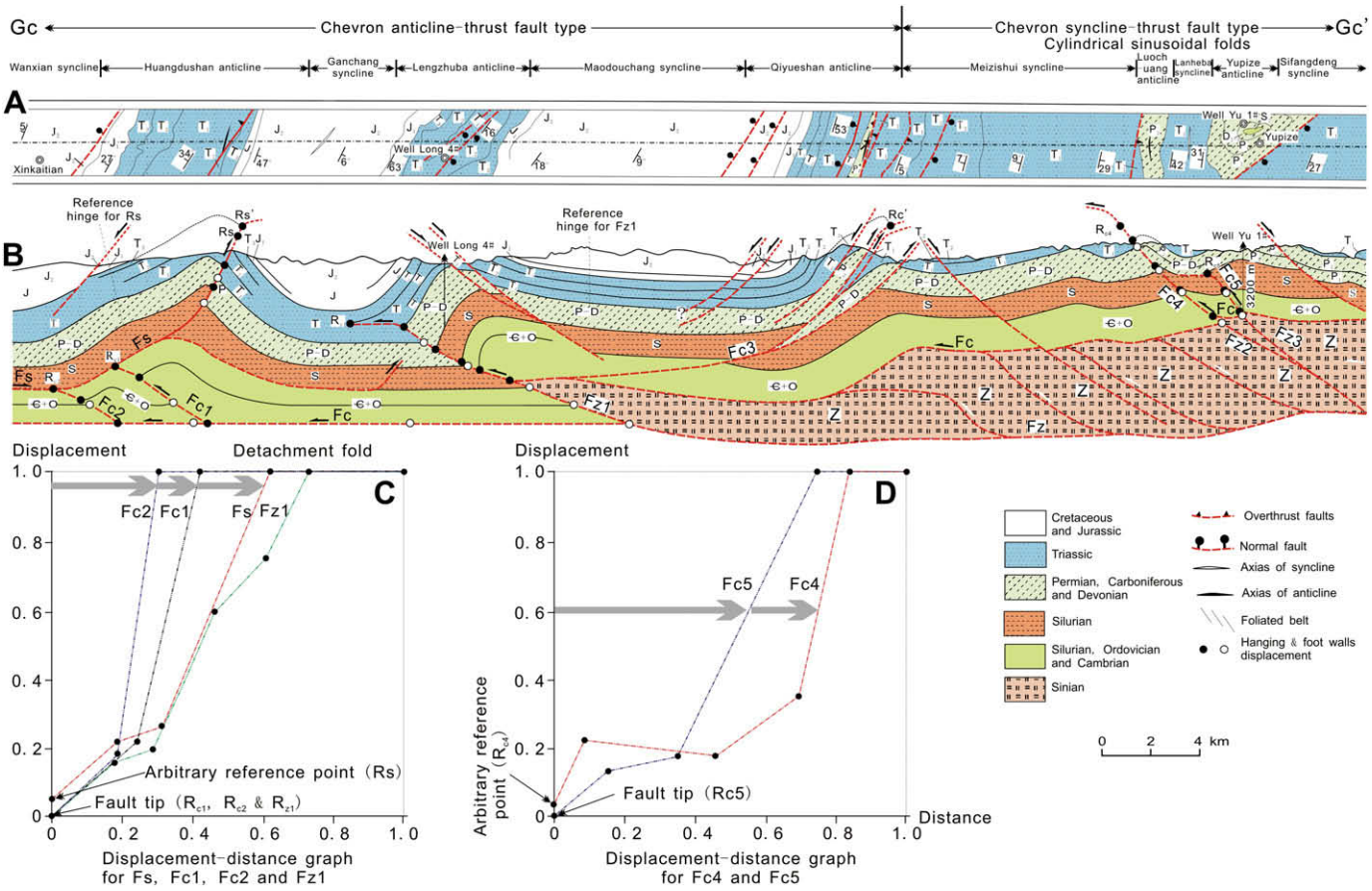

Fig. 2. (A) Strip geological map of a belt from Xinkaitian to Yupize, and (B) the corresponding geological section, which cuts through the chevron anticline-box syncline (CABS); (C) displacement–distance graph for the detachment faults Fs, Fc1, Fc2 and Fz1 in B; (D) displacement–distance graph for the detachment faults Fz2 and Fz3 in B.

thrust fault. To the southeast, the thin-skinned fold belt is separated from a thick-skinned thrust belt by the Dayin boundary detachment fault. Jurassic red-beds and volcanic rocks rest unconformably on older rocks in the thick-skinned belt (Yan et al., 2003a) (Fig. 1).

In the thin-skinned, fault-related fold belt within the Yangtze Block, the Qiyue thrust fault separates chevron anticline-thrust fault type folds to the northwest from chevron syncline-thrust fault type folds to the southeast (Figs. 1 and 2). The fold axes and faults strike northeast in the south, east–northeast in the north, and east or east–southeast close to the foreland of the Qinling-Dabie orogenic belt (Zhang et al., 1996) (Fig. 1). Individual fold axes have lengths ranging from 50 to 200 km and are arranged in a right stepping, *en-echelon* fashion (Yan et al., 2003a).

The chevron anticline-thrust fault deformation occurs in a belt bounded by the Huayun fault to the northwest and the Qiyue fault to the southeast (Fig. 1). The Triassic strata forming the cores of anticlines occur as poorly exposed thin bands, whereas Cretaceous rocks in the cores of synclines occur as well-exposed wide bands, indicating a fold system in which the anticlines form chevron folds and the synclines box folds. A few outcropping and many blind thrust faults, interpreted as flat-ramp type based on seismic data (Fig. 3), are associated with the anticlines (Yan et al., 2003a) (Fig. 1).

Toward the southeast, the anticlines have a box form with two symmetrical hinges, whereas synclines are chevron shaped with a single fold hinge. The anticlines have Paleozoic to Sinian strata in their cores, whereas the synclines have Permian to Devonian strata. The major blind faults dip to the southeast, but there are numerous second-order backthrusts (Fig. 2) (Yan et al., 2003a).

There is a gradual change from chevron anticline-thrust fault type deformation to chevron syncline-thrust fault type deformation, which is represented by cylindrical sinusoidal folds (i.e., type 1B, Ramsay and Huber, 1987) with almost the same wavelength for syncline and anticline (Yan et al., 2003a).

The thick-skinned belt structurally overlies the thin-skinned belt and is characterized by a number of klippen including the Xuefeng and Wuling nappes (Fig. 1) (Yan et al., 2003a).

The structural pattern of this thrust system in South China was previously explained by a model involving detachment faulting along various stratigraphic layers at different stages of evolution (Yan et al., 2003a; Zhang et al., 2006).

3. Equations to estimate the geometry and depth of blind faults

Interpretation of the seismic section (Fig. 3) and geological map (Fig. 2) indicates a flat-ramp-flat type for the detachment faults with a short steep forelimb of the propagation anticline and syncline–anticline–syncline arrangement in the backlimb. The geological section Gc–Gc′ suggests detachment folding to the south as well (Fig. 2). Thus, a single geometric model (Fig. 4) encompassing detachment folding as an end member (modified after Chester and Chester, 1990 and Marrett and Bentham, 1997) is used in this paper.

In this geometric model, the trigonometry relating a flat-ramp detachment fault and a hanging-wall fault-propagation fold (Fig. 4) was analyzed by Marrett and Bentham (1997) with Eqs. (1)–(3):

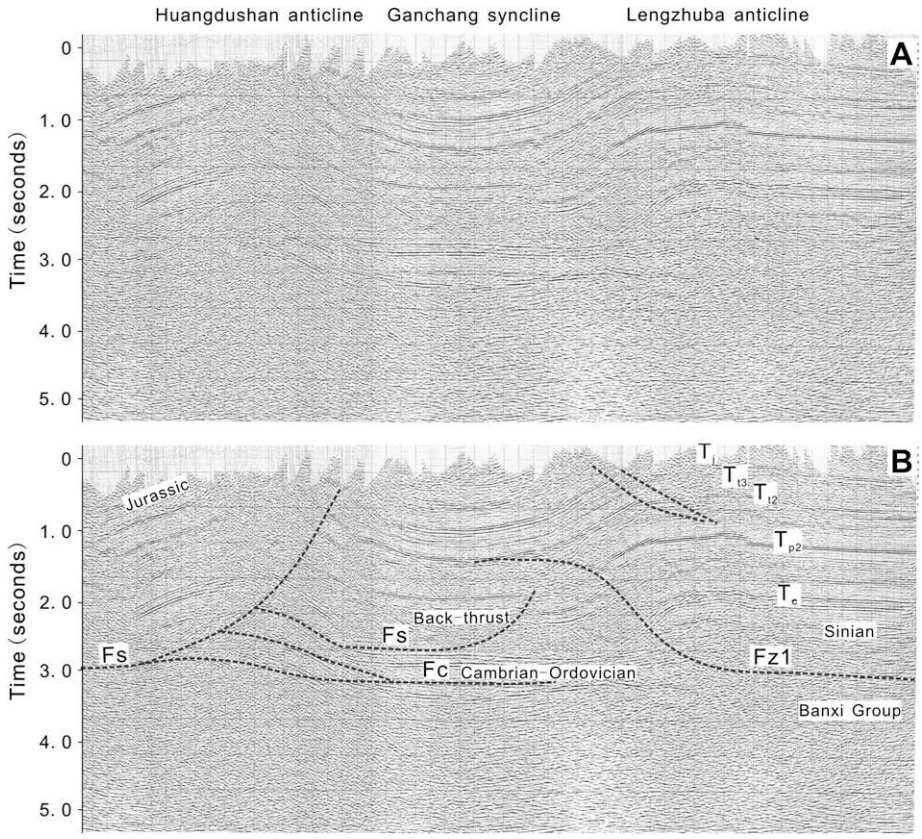

Fig. 3. (A) A time migrated seismic profile (CPCC Line 87-184); (B) interpretation for CPCC Line 87-184. T_j, T_{t3}, T_{t2}, T_{p2} and T_ε indicate the refractions of the bottom of Jurassic, upper Triassic, middle Triassic, upper Permian and Cambrian.

$$\alpha = a\cot\left[-A-B+\sqrt{(A+B)^2+2A\cot(2\theta+\gamma)-\left(\frac{t_f}{t}\right)^2}\right]$$
$$A\equiv\tan\theta-\frac{1}{2}\left[\left(\frac{t_f}{t}\right)^2+1\right]\cot\gamma-\frac{t_f}{t}\csc\gamma \quad (1)$$
$$B\equiv\frac{1}{2}\left[\left(\frac{t_f}{t}\right)^2-1\right]\cot(2\theta+\gamma)$$

$$TP = hC\csc(2\theta+\gamma-\alpha) \quad (2)$$

$$f_0 = hC\left[\frac{t}{t_f}\csc\alpha-\csc(2\theta+\gamma-\alpha)\right]$$
$$C\equiv\frac{\csc(2\theta+\gamma)}{\frac{t}{t_f}\csc\gamma+\cot\gamma-\cot(2\theta+\gamma-\alpha)} \quad (3)$$

where γ = interlimb angle; 2θ = backlimb dip; h = structural relief; t_f/t = thickness-change ratio of layering within the forelimb of the hanging-wall fold of an anticline. α = ramp dip angle; P = fold initiation point, which marks the location at which displacement begins to decrease and the fault tip point, T, occurs where displacement reaches zero. Both the P and T points define the fault-parallel distance (TP).

Using a similar geometrical model, Chester and Chester (1990) developed an Eq. (4):

$$\tan\alpha^* = \frac{1}{\left(t_f/t\right)\csc(2\theta+\gamma)+\cot(2\theta+\gamma)} \quad (4)$$

Using Eqs. (1)–(4) and the geometry and trigonometry in Fig. 4, we develop the following equations to express the depth (point L in Fig. 2) of the blind thrust fault:

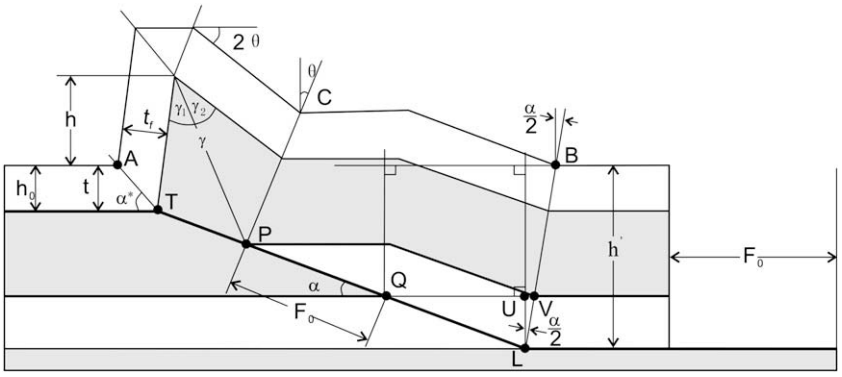

Fig. 4. Geometry of a fault-propagation/detachment fold (modified after Chester and Chester, 1990 and Marrett and Bentham, 1997).

$$QV = AB - \frac{h_0}{\tan\alpha^*} - (TP + f_0)\cos\alpha - [h_0 + (TP + f_0)\sin\alpha]\tan\left(\frac{\alpha}{2}\right) \quad (5)$$

where α^* = dip of the hinge from the forelimb to the undeformed layer; h_0 = thickness of uppermost outcrop layer; AB = outcrop width of hanging-wall anticline.

In the case of $t_f/t = 1$, i.e., no layer thickness changes within the forelimb of the hanging-wall anticline:

$$QU = \frac{QV \times \tan\left(\frac{\pi}{2} - \frac{\alpha}{2}\right)}{\tan\alpha + \tan\left(\frac{\pi}{2} - \frac{\alpha}{2}\right)} = \frac{QV \times \cot\frac{\alpha}{2}}{\tan\alpha + \cot\frac{\alpha}{2}} \quad (6)$$

$$LU = QU \times \tan\alpha \quad (7)$$

If points A and B are exposed, the depth of point L (h'), which indicates the depth of the lower flat segment of the detachment fault, can be expressed as

$$h' = h_0 + (TP + f_0) \times \sin\alpha + LU \quad (8)$$

Thus, if anticline parameters 2θ, γ, h, h_0, AB and t_f/t are known, Eqs. (1)–(3) are sufficient to obtain parameters, α, f_0 and TP, and Eqs. (4)–(8) are sufficient to obtain parameter, h', for a blind detachment fault and the associated style of detachment and fault-propagation folding.

4. Structural styles and blind detachment fault parameters of the thin-skinned thrust belt

A cross-section (Gc–Gc′) through both the chevron anticline-thrust fault zone and the northwestern part of the chevron syncline-thrust fault zone was established from field observation, magnetotelluric sounding (Yuan and Egorov, 2000), drill holes and seismic data (Fig. 2).

Fold parameters of each layer, including backlimb dip direction, dip angle (2θ), and interlimb angle (γ) were measured systematically (Table 1). The fault ramp angle (α) can be calculated from Eq. (1) using both 2θ and γ, or estimated from Fig. 5A. Integrating α with observations of locally outcropping faults, the fault geometry can be determined in the cross-section Gc–Gc′ (Figs. 2, 5 and 6).

The measured data in the section can be used to calculate the detachment fault ramp angle (α), fault displacement (f_0) and the shortening rate, distance between the fault tip and fault initiation point (TP) (Fig. 5), and lower fault flat depth (L) (Table 2), which permit reliable estimates of the fault geometry. The fold–fault assemblage can be clearly established (Fig. 2).

4.1. Structural styles of the chevron anticline-thrust fault belt

The alternating chevron anticlines and box synclines from northwest to southeast in the section include the Wanxian syncline, Huangdushan anticline, Ganchang syncline, Lengzhuba anticline, Madouchang syncline and Qiyueshan anticline (Fig. 2). Thrust faults, including locally exposed Fs, Fz1 and Fz3, and blind faults Fc1, Fc2 and Fc are identified (Fig. 2A and B).

4.1.1. The Huangdushan, Lengzhuba and Qiyueshan anticlines

The Huangdushan chevron anticline has Triassic strata in the core and Jurassic strata on the limbs (Fig. 2A and B). This anticline, separated from the Ganchang box syncline to the southeast by a locally outcropping, northwest-dipping, thrust fault (Fs), gradually changes into the Wanxian box syncline to the northwest. Fault Fs has a very small displacement, and was previously interpreted as a backthrust (Fig. 8) (Yan et al., 2003a). The increasing displacement along the ramp, constant displacement along the flat portion, and the position of the arbitrary reference point Rs off, but near, the point of origin in the displacement–distance graph (Fig. 2C) are all indicative of a propagation fold over a flat-ramp type thrust fault. Rs is thus inferred to be a denuded fault tip point for the fault (Fs).

Seismic data reveal a blind imbricated fault–fold system in the footwall of Fs. This system is composed of fault-propagation folds over imbricated thrust faults, flat-ramp-flat type Fc1 and Fc2, along the detachment fault at the bottom of the fault ramp, with constant maximum displacement in the flat portion, and the fault tip (R) at the point of origin (0,0) (Fig. 2B and C). The constant maximum displacement along the flat portion of the fault forms the detachment syncline (Marrett and Bentham, 1997), i.e., the Ganchang box syncline.

The Lengzhuba anticline has Triassic strata in the core and asymmetric limbs of Jurassic strata (Fig. 2A and B). Seismic imaging (Fig. 3) shows a blind thrust fault (Fz1) with a southeast-dipping flat-ramp-flat style. The lower flat portion lies along the base of the Sinian strata, whereas the upper flat segment lies along the base of the upper Triassic strata (Ft) (Fig. 3). Thus, the Lengzhuba fold is identified as a propagation anticline over detachment fault Fz1, which has constant maximum displacement in the flat portion, and the fault tip (R) at the point of origin (0,0) (Fig. 2B and C). In the footwall of Fz1, horizontal Cambrian–middle Triassic strata form the core of the Ganchang box syncline. Several east-dipping, high-angle, normal faults cross-cut the Lengzhuba anticline and the thrust system. The Ganchang syncline is identified as a detachment fold along fault Fc.

The Qiyueshan chevron anticline has a core of Permian strata and limbs of Triassic strata. This anticline is asymmetric with the northwestern limb being much steeper than the southeastern limb. It is separated from the Meizishui syncline of the chevron syncline-thrust fault type by at least three exposed, northwest-dipping, imbricate thrust faults (Fig. 2A and B). These faults place upper Permian over lower Triassic strata and lower Triassic over middle to lower Triassic strata (Figs. 2A, B and 7A). These faults are marked by tectonic breccia and gouge and have NE–SW-oriented scratch/mineral lineations (Figs. 2A, B and 7B, C). In the northwestern limb, variable but generally steeply-dipping Lower Triassic strata form "Z"-type second-order folds (Fig. 7D), and farther to the northwest, the fold gradually changes to the Madouchang box syncline (Fig. 2A and B). At depth, the thrust fault gradually merges into the flat segment of the fault along the base of the Cambrian strata (Fc3) (Fig. 2B). The flat portion of Fc3 extends northwestward and convergences with Fz1, and thus, the gently dipping Sinian to Ordovician strata form a wedge structure between Fc3 and Fz1 in the footwall of Fc3 (Fig. 2B). Therefore, the Qiyueshan chevron anticline-fault system is very likely the top of a structural wedge fed from displacement leaking out from the higher detachment level to the south.

4.1.2. The chevron anticline-thrust fault belt

In the displacement–distance graphs (Fig. 2C and D), all thrust faults, Fs, Fc1, Fc2 and Fz1, have increasing displacement in the ramp, and have constant displacement in the flat segment, and a fault tip (R) at, or near, the point of origin, indicating their relationship to propagation folds in the Huangdushan, Lengzhuba and Qiyueshan anticlines.

Parameters for the Huangdushan, Lengzhuba and Qiyueshan anticlines were measured from outcrops and the seismic section. These parameters include the dip direction and dip angle (2θ) of the backlimb and the interlimb angle (γ) (Tables 1 and 2). A plot of the backlimb dip vs. interlimb angle nomograms (Marrett and Bentham, 1997) gives the blind propagation anticline-related fault

Table 1
Data for the parameters of anticlines.

Strata	Backlimb dip (2θ)		Ramp angle (α)	Interlimb angle (γ)	Backlimb dip (2θ)		Ramp angle (α)	Interlimb angle (γ)	Backlimb dip (2θ)		Ramp angle (α)	Interlimb angle (γ)
	Dip direction	Dip angle			Dip direction	Dip angle			Dip direction	Dip angle		
Huangdoushan anticline					*Lengzhuba anticline*				*Qirueshan anticline*			
Jurassic	303	35	38	94	150	25	41	112	350	42	Denudated	No valid measurements
	343	32	37	96	134	20	41	108	342	73		
	337	35	39	98	127	19	41	103	340	40		
	318	21	40	101	119	26	43	105	0	39		
	0	19	40	99	127	24	42	104	342	73		
	303	35	34	89	145	17	49	111	330	80		
	343	40	50	113	141	24	40	100	336	42		
	347	17	43	106	154	29	40	98	340	50		
	345	34	40	102	160	26	35	85	330	45		
	327	25	41	103	160	23	40	109	352	52		
	315	42	45	98	177	23	48	112	332	44		
	330	30	35	88	176	29	41	100	335	51		
	328	32	39	95					324	49		
	330	30	39	97								
	345	26	37	92								
	340	39	36	93								
	331	30	40	95								
	341	32	40	99								
	348	31										
	345	32										
	345	32										
	324	34										
	345	26										
	340	28										
	342	28										
	335	22										
	356	24										
	4	21										
	350	23										
Triassic	331	44	42	99	162	35	49	110	320	40	58	125
	335	52	41	97	150	33	51	115	320	55	53	118
	295	38	47	106	152	28	50	112	320	58	60	114
	12	14	42	99	144	30	51	115	320	55	55	120
	257	3	45	98	147	24	51	117	320	44	59	124
	257	11	40	94	149	26	51	117	324	49	48	109
	350	25	40	99	131	25	48	110	335	52	55	119
	3	64	48	106	144	25	50	106	327	32	51	116
	343	79	50	100	140	22	46	107	315	19	46	109
	340	25	40	97	133	20	46	109	324	17	54	121
					129	21	52	119	350	5	55	122
					126	22	37	90	355	5	52	117
					110	20	38	96				
					147	18	39	95				
					150	17	48	110				
					155	27	48	112				
					167	22	39	97				
					160	18	40	99				

(*continued on next page*)

Table 1 (*continued*)

Strata	Backlimb dip (2θ)		Ramp angle (α)	Interlimb angle (γ)	Backlimb dip (2θ)		Ramp angle (α)	Interlimb angle (γ)	Backlimb dip (2θ)		Ramp angle (α)	Interlimb angle (γ)
	Dip direction	Dip angle			Dip direction	Dip angle			Dip direction	Dip angle		
Permian–Devonian					110	18	41	103	305	59	60	122
					147	17	44	105	322	55	53	115
					150	22	42	102	320	52	55	117
					155	26	45	106	316	45	52	118
					157	31	47	109	310	45	52	118
									306	34	56	119
									335	52	56	121
Cambrian–Silurian (southern section of Qiyueshan anticline)									345	48	45	106
									85	58	51	110
									60	56	43	103
									350	46	45	105
									315	65	50	107
									45	64	50	108
									350	67	50	105
									320	57	49	107
									355	52	49	108
									320	60	50	108
									326	66	49	105
									320	60	43	100
									324	58	48	105
									322	33	41	101
									320	66	44	99
									340	67	45	98
									320	65	48	106
									312	62	47	104
									331	70	49	102
									332	69	49	103
									334	58	46	102

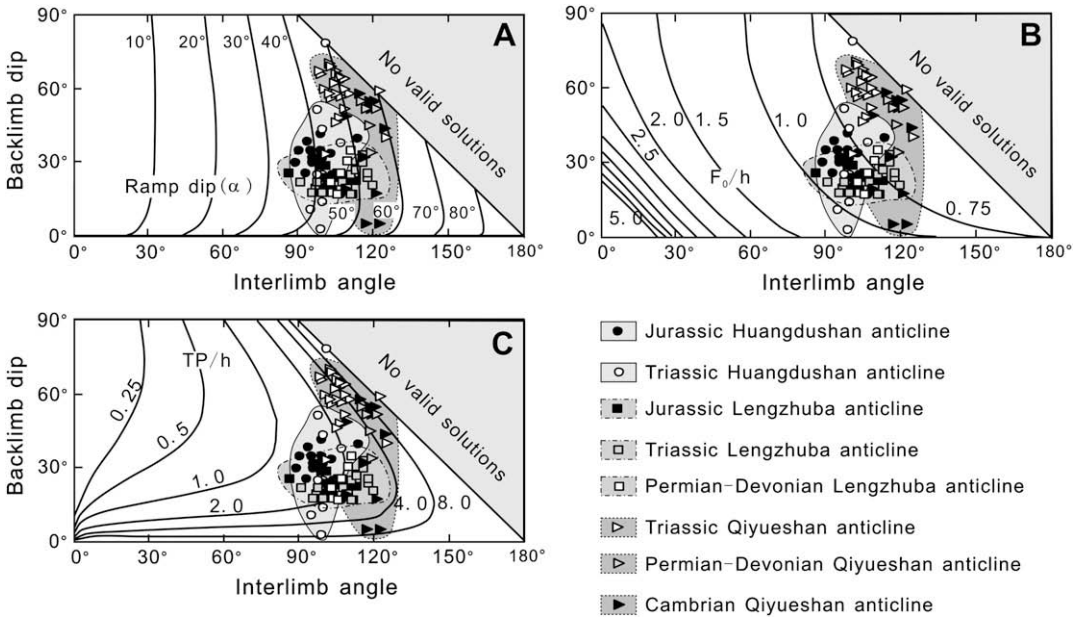

Fig. 5. Plots of the parameters of Huangdushan, Lengzhuba and Qiyueshan anticlines in nomograms of backlimb dip (2θ) vs. interlimb angle (γ) assuming that $t_f/t = 1$. (A) Ramp dip t; (B) normalized fault displacement (f_0/h); (C) normalized distance between the fault tip and the fold initiation point (TP/h) (Marrett and Bentham, 1997). Plotted data are from Table 1. Stippled area of the graph corresponds to the various combinations of input parameters that cannot result in a meaningful fold geometry.

parameters, including ramp dip (α) (Fig. 5A and Table 1), normalized fault displacement (f_0/h) and normalized distance between the fault tip and fault initiation point (TP/h) (Fig. 5B and C). The α values of 34–50° (average = 41°), 35–42° (average = 44°) and 41–60° (average = 51°) (Fig. 5A) suggest a medium dip angle for the ramp of the thrust faults. The TP/h values of 1.3–8.0, 1.2–3.8 and 2.0–8.0 for the three faults (Fig. 5C) indicate that limited increasing displacement is sensitive to a small range of interlimb angle, whereas the backlimb dip is variable (Fig. 5B and C) for a given structural relief.

The plot of ramp dip angle vs. backlimb dip angle (Fig. 6) gives $t_f/t = 1$, or slightly less than 1, in the case of larger interlimb angle ($\gamma = 90°$ or greater), implying no or very little forelimb thickness change (Marrett and Bentham, 1997). Using the lower Triassic strata as a marker, the parameters for the Huangdushan, Lengzhuba and Qiyueshan anticlines are measured or estimated relative to the referenced hinges of Fs, Fz1 and Fc3, respectively (Fig. 2; Table 2). The h' values of 4.9, 7.4 and 4.4 km for the Huangdushan, Lengzhuba and Qiyueshan anticlines, respectively, roughly correspond to depths of the Silurian, Sinian and Cambrian strata in the anticlines and thus indicate that the detachment faults (bottom flat) lie along the bottom of Silurian, Sinian and Cambrian (Fc3) strata, respectively. The α values of 41.6°, 45° and 49.5° for the three anticlines, respectively, are consistent with the average results from the projection in Fig. 5A, and indicate moderate dip angles for the fault ramp. $f_0 = 0.63$, 2.38 and 1.16 km for the three anticlines indicating a shortening of about 9%, 19.2% and 17.5% ($f_0/(AB + f_0) \times 100\%$), respectively, for the anticlines; TP values of 1.26 km, 5.95 km and 3.92 km, respectively, indicate small to medium values of the fault-parallel distance from point P to the blind fault tip point R (Fig. 2B) in the displacement–distance graph (Fig. 2C).

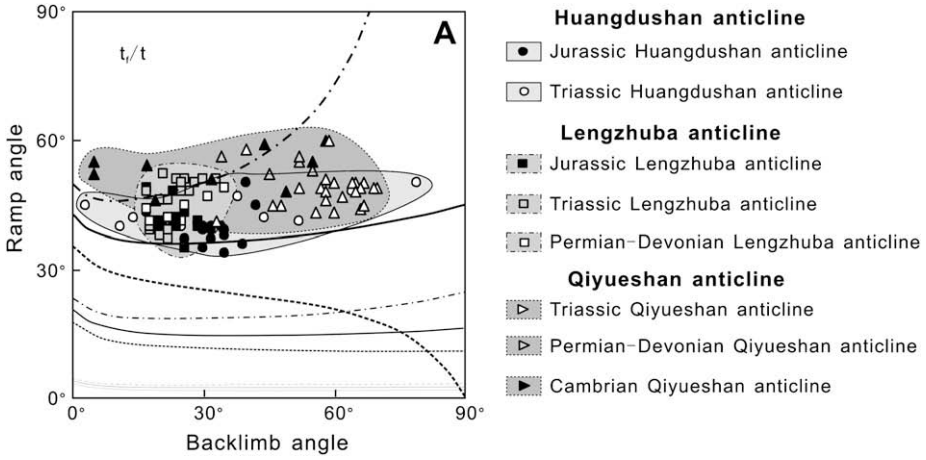

Fig. 6. Plots of backlimb dips (2θ) vs. ramp dip (α) for the Huangdushan, Lengzhuba and Qiyueshan anticlines showing the forelimb thickness-change ratios (t_f/t). Thin curves correspond to $\gamma = 10°$; medium curves correspond to $\gamma = 45°$; bold curves correspond to $\gamma = 90°$. Continuous curves correspond to $t_f/t = 1$; dashed curves correspond to $t_f/t = 1.25$; dashed-dotted curves correspond to $t_f/t = 0.8$ (after Marrett and Bentham, 1997). Plotted data are from Table 1. Stippled area of the graph corresponds to the various combinations of input parameters that cannot result in a meaningful fold geometry.

Table 2
Parameters input of the anticlines and output of the detachment fault.

Lower Triassic mark layer	Input parameters of the anticline						Output results of the detachment fault				
	2θ	γ	h	h_0	AB	t_f/t	α	f_0	$f_0/(f_0+AB)$	TP	h'
Units	Degree		km				Degree	km	%	km	
Huangdushan anticline	31	99	0.8	1.4	6.4	1	41.6	0.6	9.0	1.3	4.9
Lengzhuba anticline	24	106	3.0	0.8	10.0	1	45.0	2.4	19.2	6.0	7.4
Qiyueshan anticline	38	111	1.7	0.4	5.5	1	49.5	1.2	17.5	3.9	4.4
Yupize anticline	19	125	0.6	1.2	3.7	1	56.3	0.4	10.7	2.2	3.4

4.2. Structural styles and parameters of the chevron syncline-thrust fault belt

In the southeastern part of the geological section Gc–Gc′, cylindrical sinusoidal folds include the Meizishui syncline, Luochuang anticline, Lanheba anticline, Yupize anticline and Sifangdeng syncline. Several thrust faults, including locally exposed Fc4 and Fc5, were identified (Fig. 2A and B). Several exposed normal faults cross-cut the thrust fault–fold system with brittle deformational characteristics and indicate late Cretaceous to Tertiary extensional tectonics (Fig. 2).

The thrust fault Fc4 has a dip angle (α) of 53°, and cuts the small hanging wall of the Luochuang anticline, which is separated from the relatively large-scale Yupize anticline by the Lanheba syncline (Fig. 2A and B). Both anticlines and synclines are cylindrical sinusoidal folds with single hinges (i.e., type 1B of Ramsay and Huber, 1987), indicating a gradual change in the structural style from chevron anticlines to chevron synclines (Yan et al., 2003a). In well Yu 1#, the Yupize anticline is likely to be a hanging-wall propagation fold of the blind thrust fault Fc5, which is inferred to have a flat-ramp-flat style with the upper flat segment located along the boundary between the Silurian and Devonian strata. Thus, the Luochuang anticline is probably a propagation fold of Fc4 whose upper flat has been eroded, and the Lanheba syncline formed over the upper flat segment of Fc5. We interpret both Fc4 and Fc5 as parts of an imbricate thrust fault system (Fig. 2B).

Parameters for the Yupize anticline, measured from field observations and data from well Yu 1#, are used to estimate the detachment fault parameters (Table 2). Using the Silurian strata as a marker, the parameters of the Yupize anticline were estimated with reference to point Rc4 of Fc5 (Fig. 2). The parameters include 2θ°, γ, h, h_0, and AB assuming $t_f/t = 1$ (Table 2). Using these values and the Eqs. (1)–(8) (Table 2), the blind fault parameters are calculated (Table 2).

A value of $h' = 3.4$ km indicates that the detachment fault occurs along the base of the Cambrian strata, and a value of $\alpha = 56°$ suggests a steeper dip for the fault ramp than that in the chevron fold–fault type belt. $f_0 = 0.44$ km is the shortening distance and indicates about 10.7% shortening for this fold; $TP = 2.2$ km indicates the fault-parallel distance from point P to the fault tip point Rc5 (Fig. 2B and D).

Both Fc4 and Fc5 have increasing displacement along the ramp and then constant displacement along an inferred flat at depth, but

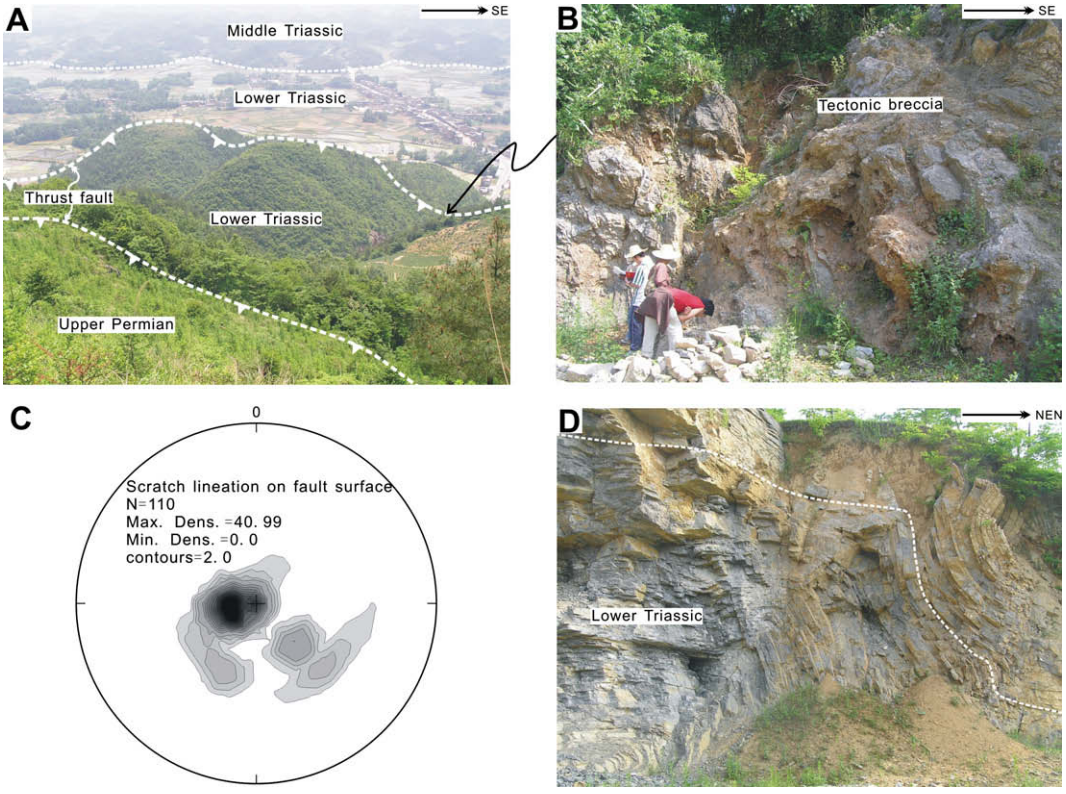

Fig. 7. Field pictures of the Qiyueshan anticline: (A) northwest-dipping imbricate thrust faults in the southeastern limb of the Qiyueshan anticline; (B) tectonic breccia within the thrust fault; (C) lower-hemisphere stereo-projection of mineral lineations or scratches on the fault plane; (D) "Z"-type folds of lower Triassic strata resulted by variable dip angles in the northwestern limb.

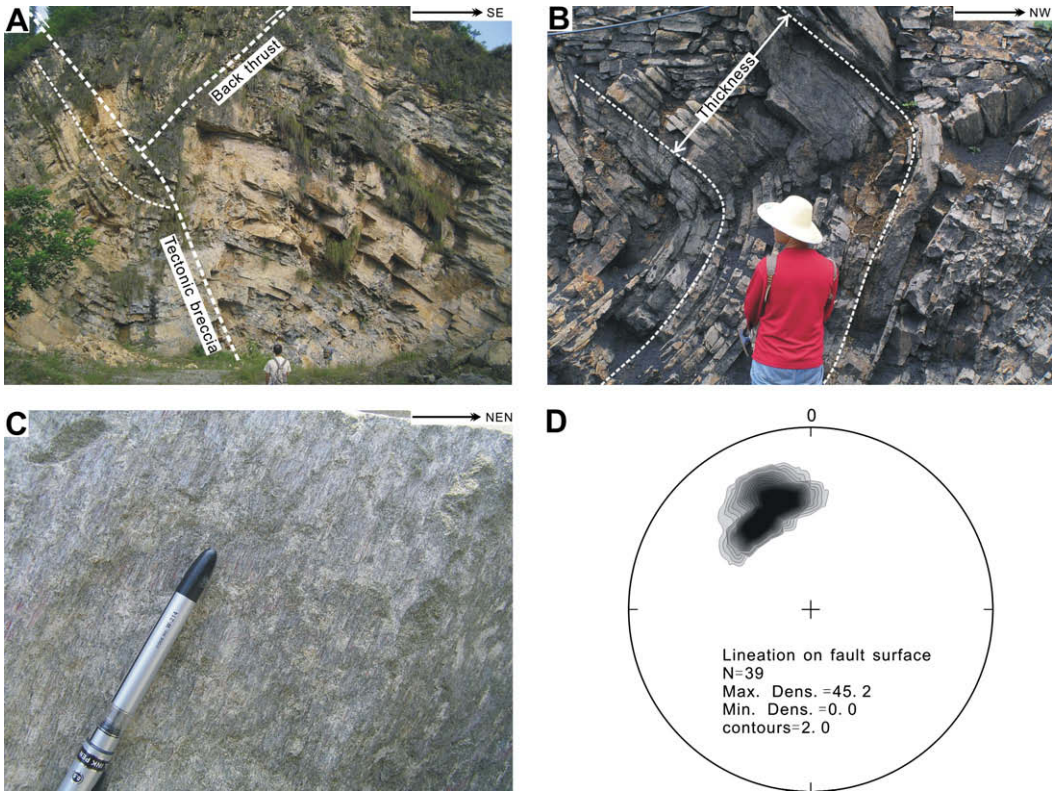

Fig. 8. Field pictures of the Huangdushan anticline: (A) a thrust fault with tectonic breccia and corresponding backthrust fault occur in lower Triassic strata; (B) folded lower Triassic limestone with thickness-change ratio $t_f/t = 1$ within the forelimb; (C) oriented calcite crystal on the surface of the backthrust; (D) lower-hemisphere stereo-projection of mineral lineations or scratches.

Fc4 has an arbitrary reference point Rc4 near the point of origin, while Fc5 has a tip point at the point of origin (Fig. 2D).

In the footwall of Fc (the composite Fc4 and Fc5), a duplex thrust system composed of Sinian slices and imbricated thrust faults is inferred from the uplifted Sinian strata (Fig. 2B).

5. Discussion

5.1. Depth and geometry of the detachment fault

The fault-propagation fold parameters (2θ, γ, h, h_0, AB and t_f/t) can be used to calculate the blind fault parameters of α, f_0, h' and TP according to the Eqs. (1)–(8). These fault parameters are sufficient to constrain the exact location, geometry and, to a certain extent, the kinematic characteristics of the blind detachment fault in the thin-skinned fold-propagation model in Fig. 4. The fault data are sufficient to establish reasonable geological sections and to carry out structural analysis.

Anticline parameters from the variable fold types in the geological section Gc–Gc′ are applied to determine the geometry and depth of the detachment fault. Although there are similar geometric styles of alternating chevron and box synclines, or cylindrical sinusoidal folds in the geological section Gc–Gc′, estimation and interpretation of the fault geometry, depth and implied detachment fault–fold assemblage are variable.

On the basis of the blind fault propagation and detachment fold model (Chester and Chester, 1990; Suppe and Medwedeff, 1990; Marrett and Bentham, 1997), all the thrust faults in Fig. 2A and B, Fc1, Fc2, Fs, Fz1, Fz2 and Fz3, have increasing displacement along the ramp, constant displacement along the flat, and a reference point Rs′ near or at the point of origin in the displacement–distance graphs (Fig. 2C and D). These types of displacement–distance graphs show the characteristics of propagation folds over a flat-ramp type thrust fault, although the exact Rs points have been eroded for some of the outcropping faults. Thus, Eqs. (1)–(8) are applicable to the analysis of the faults in Fig. 2A and B.

The parameters of the Huangdushan chevron anticline indicate that the lower flat segment of the thrust fault lies at 4.9 km, exactly the base of the Silurian detachment (Fs). These parameters also indicate that this fault has a medium ramp dip angle $\alpha = 42°$, a small shortening rate of 9% and $TP = 1.26$, and a small slip displacement along the fault. Seismic sections reveal a blind imbricate thrust fault system along Fc and a buried box anticline in the footwall of the Fs (Figs. 2 and 3). The inconsistent structural style revealed by the presence of an upper chevron and a lower box anticline is the result of backthrust faults along Fs, which were produced by the northwestward imbricate thrusts (Fig. 2).

Parameters of the Lengzhuba anticline reveal a blind northwest-directed, flat-ramp-flat type thrust fault (Fz1) at 7.40 km, exactly at the base of the Sinian detachment (Fz1), and show that this fault has a medium ramp dip angle $\alpha = 45°$, a large shortening rate of 19.2% and a TP value of 5.95, which is almost 5 times that along the Fs of the Huangdushan anticline, but with smaller displacement. The horizontal lower wall of the Fz1 indicates very weak deformation in the core of the Ganchang syncline.

Parameters of the Qiyueshan anticline reveal that the thrust fault lies at a depth of 6.16 km, that the ramp dip angle $\alpha = 49.5°$, that the shortening rate was 17.5% and that $TP = 3.92$, 3 times greater than for the Fs of the Huangdushan anticline, even though the actual displacement is small. These structural characteristics resemble those in the fault–fold assemblage of the Huangdushan anticline and lead us to interpret Fc3 as a backthrust, which separates a blind imbricated thrust fault and a buried box anticline (probably along Fc, see following discussion) in the footwall of Fc3 (Fig. 2).

In the southeastern part of the Gc–Gc′ section (Fig. 2), the fold–fault assemblage is represented by the cylindrical sinusoidal Yupize anticline, which has the structural style of a propagation fold (Fig. 2D). The parameters of the Yupize anticline reveal that the lower flat depth of the thrust fault lies at 3.4 km, exactly at the base of the Cambrian detachment (Fc), and further define the geometry of the faults with a ramp dip angle $\alpha = 56^\circ$, a shortening rate of 10.6% and $TP = 2.2$, which is more than that along Fs in the Huangdushan anticline, although the amount of slip is small. The much smaller depth and variable shape of Fc imply uplift of the Sinian strata in the footwall of Fc, produced by the out-of-sequence imbricate duplex thrusting of Fz2 and Fz3 (Fig. 2B).

Previous studies have identified at least 4 potential detachment zones: the base of the Sinian strata (Fz), the Cambrian strata (Fc), the Silurian strata (Fs) and the Triassic strata (Ft) (Fig. 1B) (Yan et al., 2003a). The detachment fault Fz1, which has the largest fault depth and shortening rate, formed the broad Lengzhuba anticline, whereas southeast-directed backthrust faults, which have smaller fault depths and shortening rates, produced the Huangdushan chevron and Qiyueshan anticlines (see section Gc–Gc′). The detachment faults Fc4 and Fc5 have larger shortening rates and shallower depths than the small-scale Yupize anticline. Both Fz and Fc detachment faults produced northwest-oriented duplex imbricate thrust assemblages. All the detachment faults have a flat-ramp-flat style with ramp angles ranging from 42° to 56°, which is consistent with the conjugate angle defined by Zheng et al. (2004).

5.2. Model for development of the detachment faults and folds

In the geological section Gc–Gc′, the detachment fault along the base of the Sinian strata (Fz) dominates the multi-layer, fault-related fold system because of the lithological contrast between the Sinian strata and the basement rocks of the Banxi Group (Fig. 1B) (HBGMR2, 1988; HBGMR1, 1990; Yan et al., 2003a). The floor thrust Fz and also the roof thrust dip down the transport direction at the southeast end (Fig. 2B), related to the overall gentle northwest dip (younging) on the surface, indicating a steepening of the duplex bodies to the southeast produced by a forward propagating duplexes (Yan et al., 2003a). The stepwise progressive northwestward and upward deformation then produced the flat-ramp-flat style of detachment faulting at the base of the Cambrian (Fc), and Silurian (Fs) (Liu et al., 1994; SBGMR, 1991; Yan et al., 2003a; Wang et al., 2005, 2007) (Fig. 1B). Geometrical data and depth constraints on detachment faults provided in this paper allow a 3-stage kinematic model for the deformation (Fig. 9).

The first stage involves formation of a chevron anticline on the hanging wall by a flat-ramp-flat type thrust fault (Yan et al., 2003a) in which the fault tip is located at the inflection-point. In this case, a simple propagation fold with a chevron anticline, box syncline and blind fault tip is formed (Fig. 9A).

The second stage is the gradual change from chevron anticline to box or open anticlines as the fault tip moves away from the inflection-point along the flat, and a new chevron anticline is formed by the next ramp (Fig. 9B). In this case, the potential fault will develop into a structural wedge (the broken lines in Fig. 9B).

The final stage involves formation of the fault-related fold style. The fault–fault style depends on the final location of the detachment fault. The southeast-directed counterforce resulted in the formation of an in-sequence (forward progress) imbricated duplex within the Paleozoic strata, and led to formation of backthrusts, along the forward roof of the imbricated duplex (Boyer and Elliot, 1982) (Fig. 9C). However, within the Sinian strata, the southeastward counterforce resulted in out-of-sequence thrust faults, i.e., faults developing behind the main thrust. The out-of-sequence thrust faults have a non-planar, folded roof duplex (Boyer, 1992; Davis, 1999), which thickened and uplifted the Sinian strata (HBGMR2, 1988) and formed small-scale and cylindrical sinusoidal folds in the hanging wall of the roof thrust (Fig. 9C). The accommodation of strain between chevron anticline-thrust faulting and chevron syncline-thrust faulting led to the formation of the backthrust Fc3. The backthrusts, Fs and Fc3, cut upward and finally produced chevron anticlines in the hanging wall.

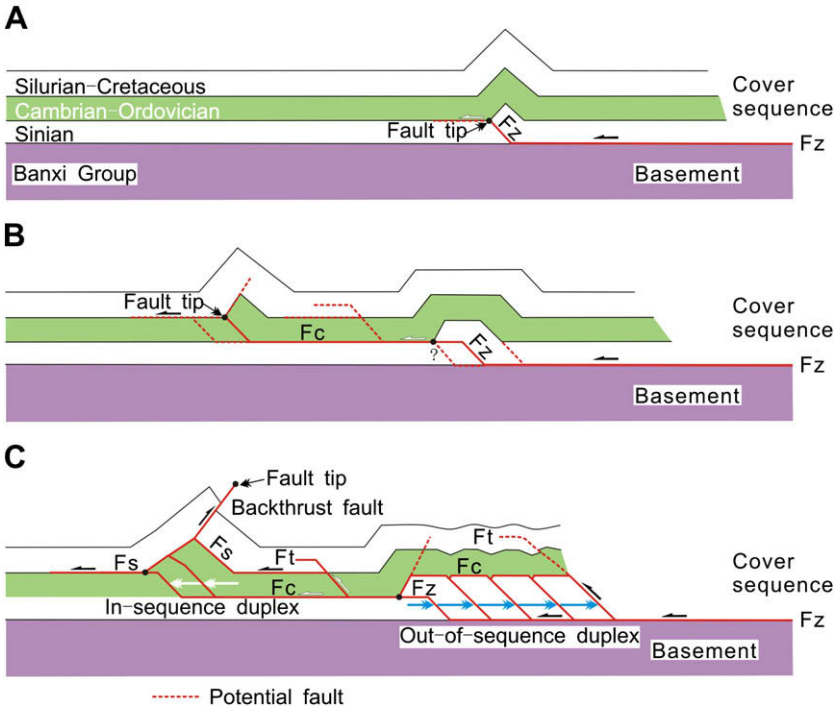

Fig. 9. A tectonic model to interpret the formation of the thin-skinned, fault-related fold belt in South China (modified on the basis of Yan et al., 2003a) (see text for discussion).

5.3. Possible origin of the Mesozoic fault-related fold belt in South China

The development of the Mesozoic detachment faults has significant implications for the origin of the Mesozoic fault–fold belt in South China. Previously Hsu et al. (1990) proposed a Mesozoic continental collision between the Yangtze and Cathaysian Blocks (inset in Fig. 1) involving overthrusting of a Mesozoic ophiolite onto the foreland thrust belt to explain the observed deformation, but this model is not well supported by the geological evidence (see Chen et al., 1991, and references therein; Yan et al., 2003b). Li and Li (2007) have recently proposed a flat-slab subduction model for Mesozoic South China to explain the development of a broad (~1300-km-wide) intra-continental orogen. This model suggests magmatic activity migrating from the coastal region (SE) into the continental interior (NW) between ca. 250 Ma and 190 Ma with the formation of a shallow-marine basin in the wake of the migrating foreland fold-and-thrust belt. However, the development of the thin-skinned, fault-related fold belt occurred during the Jurassic to Cretaceous (Yan et al., 2003a) and thus does not support this model.

Yan et al. (2003a) proposed a Mesozoic intra-continental orogeny in South China, which is further supported by our study. This event was produced by collision between the South China and North China Blocks which took place in a scissor-like fashion (Yin and Nie, 1993; Yokoyama et al., 2001) along the east–west-trending Qinling-Dabie suture zone. The onset of collision has been dated at early Triassic (~230 Ma) with a westward progression as the Yangtze Block rotated clockwise with respect to the North China Block (Zhang et al., 1996, 2006). The final collision in the west was most likely completed in the late Triassic (Mattauer et al., 1985, 1992; Zhao and Coe, 1987; Yin and Nie, 1993; Meng and Zhang, 1999; Yokoyama et al., 2001; Zhou et al., 2008). Subsequent to this final collision, the indentation of the Yangtze Block into the North China Block in the late Jurassic to early Cretaceous (Yokoyama et al., 2001) resulted in intra-continental deformation and crustal delamination (Okay and Sengor, 1992). This intra-continental deformation transported the Banxi Group northward over the Paleozoic strata. However, the age of collision was progressively younger from east to west and the northeast-trending Sichuan Basin acted as a stable part of the Yangtze Block (SBGMR, 1991) and rotated clockwise as a rigid structure during the orogeny (Yokoyama et al., 2001). Thus the vergence direction of the thrust system changed toward the northwest.

6. Conclusions

Fault-propagation fold parameters, including backlimb dip angle (2θ), interlimb angle (γ), height of anticline (h), thickness of the referenced layer (h_0), width of the anticline (AB) and thickness-change ratio of layering within the forelimb (t_f/t), can be used to constrain the depth and geometry of blind thrust faults. This technique is applied in the study of the thin-skinned, multi-layer thrust system in South China, which is characterized by chevron anticlines and synclines related to thrust faults. The chevron anticlines were formed by backthrusting and overprinting of an in-sequence imbricated duplex, whereas cylindrical sinusoidal folds were formed by thickening and uplifting of the out-of-sequence imbricated duplex.

Acknowledgements

This study was supported by research grants from the NSFC (Projects 40434011, 40621002 and 40872140), IRT0546 and the 111 Project (No. B07011) National Basic Research Program of China (2009CB421001) and China Petroleum and Chemical Cooperation (CPCC09-01). We thank P.T. Robinson for enlightening discussions and for his assistance throughout this study. We thank Prof. Ding Daogui for providing seismic data and discussions. We thank Andreas Plesch and an anonymous referee for thorough reviews that helped improve this paper and they are gratefully acknowledged.

References

Allmendinger, R., Shaw, J., 2000. Estimation of fault propagation distance from fold shape: implications for earthquake hazard assessment. Geology 28 (12), 1099–1102.
Berger, P., Johnson, A.M., 1980. First-order analysis of deformation of a thrust sheet moving over a ramp. Tectonophysics 70, T9–T24.
Boyer, S.E., Elliot, D., 1982. Thrust systems. American Association of Petroleum Geologists Bulletin 66, 1196–1230.
Boyer, S.E., 1992. Geometric evidence for synchronous thrusting in the southern Alberta and northwest Montana thrust belts. In: McClay, K.R. (Ed.), Thrust Tectonics. Chapman and Hall, London, pp. 377–390.
Chen, J., Foland, K.A., Xing, F., Xü, X., Zhou, T., 1991. Magmatism along the southeast margin of the Yangtze Block: Precambrian collision of the Yangtze and Cathaysia blocks of China. Geology 19, 815–818.
Chester, J.S., Chester, F.M., 1990. Fault-propagation folds above thrusts with constant dip. Journal of Structural Geology 12, 903–910.
Cooke, M., Pollard, D.D., 1997. Bedding-plane slip in initial stages of fault-related folding. Journal of Structural Geology 19, 567–581.
David, A.M., Simon, A.K., Lisa, M.B., 1997. Distribution of fault slip in outcrop-scale fault-related folds, Appalachian Mountains. Journal of Structural Geology 19, 257–267.
Davis, G.A., 1999. Challenging some widely held beliefs about thrust fault geometries – from field studies in the Y.S. Cordillera and Northern China. Earth Science Frontiers 6, 49–66.
Hsu, K.J., Li, J., Chen, H., Wang, Q., Sun, S., Sengor, A.M.C., 1990. Tectonics of South China: key to understanding West Pacific geology. Tectonophysics 183, 9–39.
HBGMR1 (Hubei Bureau of Geology and Mineral Resources), 1990. Regional Geology of Hubei Province. Geological Publishing House, Beijing, China, pp. 1–645 (in Chinese with English abstract).
HBGMR2 (Hunan Bureau of Geology and Mineral Resources), 1988. Regional Geology of Hunan Province. Geological Publishing House, Beijing, China, pp. 1–528 (in Chinese with English abstract).
Jamison, W.R., 1987. Geometric analysis of fold development in overthrust terranes. Journal of Structural Geology 9, 207–219.
Johnson, K., Johnson, A., 2001. Mechanical analysis of the geometry of forced-folds. Journal of Structural Geology 24, 401–410.
Kilsdonk, B., Fletcher, R.C., 1989. An analytical model of hanging-wall and footwall deformation at ramps on normal and thrust faults. Tectonophysics 163, 153–168.
Li, Z.X., Li, X.H., 2007. Formation of the 1300-km-wide intracontinental orogen and postorogenic magmatic province in Mesozoic South China: a flat-slab subduction model. Geology 35, 179–182, doi:10.1130/G23193A.1. 4 Figures; Data Repository Item 2007041.
Liu, H.F., Lian, H.S., Cai, L.G., Shen, F., 1994. Structural styles of the Longmenshan thrust belt and evolution of the foreland basin in the western Sichuan province, China. Acta Geologica Sinica 68, 101–118 (in Chinese with English abstract).
Liu, H., Li, Y., Hao, J., 1996. On the Banxi Group and its related tectonic problems in south China. Journal of Southeast Asian Earth Sciences 13, 191–196.
Liu, S.F., Steel, R., Zhang, G.W., 2005. Mesozoic sedimentary basin development and tectonic implication, northern Yangtze Block, eastern China: record of continent–continent collision. Journal of Asian Earth Sciences 25, 9–27.
Mattauer, M., Matte, Ph., Malavielle, J., Tapponnier, P., Maluski, H., Qin, Z.Q., Lu, L.Y., Tang, Q.Y., 1985. Tectonics of the Qinling belt: build-up and evolution of eastern Asia. Nature 317, 496–500.
Mattauer, M., Malavieille, J., Calassou, S., Lancelot, J., Roger, F., Hao, Z.W., Xu, Z.Q., Hou, L.W., 1992. The Songpan-Ganze Triassic belt of west Sichuan and eastern Tibet – a decollement fold belt on passive margin. Comptes Rendus de l' Academie des Sciences, Paris, II 314, 619–626.
Marrett, R., Bentham, P.A., 1997. Geometric analysis of hybrid fault-propagation/detachment folds. Journal of Structural Geology 19, 243–248.
McNaught, M.A., Mitra, G., 1993. A kinematic model for the origin of footwall synclines. Journal of Structural Geology 15, 805–808.
Meng, Q.R., Zhang, G.W., 1999. Timing of collision of the North and South China blocks: controversy and reconciliation. Geology 27, 123–126.
Mitra, S., 1990. Fault-propagation folds: geometry, kinematic evolution, and hydrocarbon traps. American Association of Petroleum Geologists Bulletin 74, 921–945.
Okay, A.I., Sengor, A.M., 1992. Evidence for intracontinental thrustrelated exhumation of the ultra-high-pressure rocks in China. Geology 20, 411–414.
Ramsay, J.G., Huber, M.I., 1987. Fold and fracture. In: The Techniques of Modern Structural Geology, vol. 2. Academic Press, pp. 347–363.
Salvini, F., Storti, F., 2001. The distribution of deformation in parallel fault-related folds with migrating axial surfaces: comparison between fault propagation and fault-bend folding. Journal of Structural Geology 23, 25–32.
Savage, H.M., Cooke, M.L., 2003. Can flat-ramp-flat fault geometry be inferred from fold shape? A comparison of kinematic and mechanical folds. Journal of Structural Geology 25, 2023–2034.
SBGMR (Sichuan Bureau of Geology and Mineral Resources), 1991. Regional Geology of Sichuan Province. Geological Publishing House, Beijing, China, pp. 1–680 (in Chinese with English abstract).

Strayer, L.M., Hudleston, P.J., 1997. Numerical modeling of fold initiation at thrust ramps. Journal of Structural Geology 19 (3–4), 551–566.
Suppe, J., 1983. Geometry and kinematics of fault-bend folding. American Journal of Science 283 (7), 684–721.
Suppe, J., Medwedeff, D.A., 1984. Fault-propagation folding. Geological Society of America, Abstracts with Programs 16, 670.
Suppe, J., Medwedeff, D.A., 1990. Geometry and kinematics of fault-propagation folding. Eclogae Geologicae Helvetiae 83, 409–454.
Wang, Y.J., Zhang, Y.H., Fan, W.M., Peng, T.P., 2005. Structural signatures and $^{40}Ar/^{39}Ar$ geochronology of the Indosinian Xuefengshan transpressive belt, south China interior. Journal of Structural Geology 27, 985–998.
Wang, Y.J., Fan, W.M., Cawood, P.A., Ji, S.C., Peng, T.P., Chen, X.Y., 2007. Indosinian high-strain deformation for the Yunkaidashan tectonic belt, south China: kinematics and $^{40}Ar/^{39}Ar$ geochronological constraints. Tectonics 26, TC6008, doi:10.1029/2007TC002099.
Wickham, J., 1995. Fault displacement-gradient folds and the structure at Lost Hills, California (U.S.A.). Journal of Structural Geology 17, 1293–1302.
Wilkerson, M.S., Medwedeff, D.A., Marshak, S., 1991. Geometrical modeling of fault-related folds: a pseudo-three-dimensional approach. Journal of Structural Geology 13, 801–812.
Xiao, W.J., He, H.Q., 2005. Early Mesozoic thrust tectonics of the northwest Zhejiang region (Southeast China). Geological Society of America Bulletin 117, 945–961.
Yan, D.P., Zhou, M.F., Song, H.L., Wang, X.W., Malpas, J., 2003a. Origin and tectonic significance of a Mesozoic multi-layer over-thrust system within the Yangtze Block (South China). Tectonophysics 361, 239–254.
Yan, D.-P., Zhou, M.-F., Song, H.L., Fu, Z.R., 2003b. Structural style and tectonic significance of the Jianglang dome in the eastern margin of the Tibetan Plateau, China. Journal of Structural Geology 25, 765–779.
Yan, D.P., Zhou, M.F., Wang, C.Y., Xia, B., 2006. Structural and geochronological constraints on the tectonic evolution of the Dulong-Song Chay tectonic dome in Yunnan province, SW China. Journal of Asian Earth Sciences 28, 332–353.
Yan, D.P., Zhou, M.F., Wei, G.Q., Gao, J.F., Liu, S.F., Xu, P., Shi, X.Y., 2008. The Pengguan tectonic dome of Longmen Mountains, Sichuan Province: Mesozoic denudation of a Neoproterozoic magmatic arc-basin system. Science in China, Series D: Earth Sciences 51, 1545–1559.
Yin, A., Nie, S., 1993. An indentation model for North and South China collision and the development of the Tanlu and Honam fault systems, eastern Asia. Tectonics 12, 801–813.
Yuan, X.C., Egorov, A., 2000. Arctic Ocean–Eurasia–Pacific Ocean geoscience transect (1:1 000 000) (Chinese section). Publication No. 276 of the International Lithosphere Program: GGT 21. Science Press, Beijing (in Chinese).
Yokoyama, M., Liu, Y., Halim, N., Otofuji, Y.I., 2001. Paleomagnetic study of the Upper Jurassic rocks from the Sichuan basin: tectonics aspects for the collision between the Yangtze Block and the North China Block. Earth and Planetary Science Letters 193, 273–285.
Zhang, G.W., Meng, Q.R., Yu, Z.P., Sun, Y., Zhou, D.W., Guo, A.L., 1996. Orogenesis and dynamics of the Qinling orogen. Science in China, Series D: Earth Sciences 39, 225–234.
Zhang, K.J., Cai, J.X., Zhu, J.X., 2006. North China and South China collision: insights from analogue modeling. Journal of Geodynamics 42, 38–51.
Zhang, S.H., Jiang, G.Q., Dong, J.N., Han, Y.G., Wu, H.C., 2008. New SHRIMP U–Pb age from the Wuqiangxi formation of Banxi Group: implications for rifting and stratigraphic erosion associated with the early Cryogenian (Sturtian) glaciation in South China. Science in China, Series D: Earth Sciences 51, 1537–1544.
Zhao, X., Coe, R.S., 1987. Palaeomagnetic constrains on the collision and rotation of North and South China. Nature 327, 141–144.
Zheng, Y.D., Wang, T., Ma, M.B., Davis, G.A., 2004. Maximum effective moment criterion and the origin of low-angle normal faults. Journal Structural Geology 26, 271–285.
Zhou, M.F., Yan, D.P., Kennedy, A.K., Li, Y., Ding, J., 2002. SHRIMP U–Pb zircon geochronological and geochemical evidence for Neoproterozoic, arc-magmatism along the western margin of the Yangtze Block, South China. Earth and Planetary Science Letters 196, 51–67.
Zhou, M.F., Yan, D.P., Vasconcelos, P.M., Li, J.W., Hu, R.Z., 2008. Structural and geochronological constraints on the tectono-thermal evolution of the Danba domal terrane, eastern margin of the Tibetan plateau. Journal of Asian Earth Sciences 33, 414–427.